The role of weak interactions in lignin polymerization

Citation: Sánchez-González, Ángel, Francisco J. Martín-Martínez, and J. A. Dobado. "The Role of Weak Interactions in Lignin Polymerization." Journal of Molecular Modeling 23.3 (2017): n. pag.

As Published: http://dx.doi.org/10.1007/s00894-017-3257-4

Publisher: Springer Berlin Heidelberg

Persistent URL: http://hdl.handle.net/1721.1/107002

Version: Author's final manuscript: final author's manuscript post peer review, without publisher's formatting or copy editing

Noname manuscript No.
(will be inserted by the editor)

The role of weak interactions in lignin polymerization

Ángel Sánchez-González · Francisco J. Martín-Martínez* · J. A. Dobado

Received: date / Accepted: date

Abstract Lignin is the most abundant natural polymer composed by aromatic moieties. Its chemical composition and its abundance have focused efforts to unlock its potential as a source of aromatic compounds for many years. The lack of a proper way for lignin de-polymerization has hampered its success as natural solution for commodity aromatic chemicals, which is also due to the lack of understanding of the underlying mechanisms of lignin polymerization. A fuller fundamental understanding of polymerization mechanisms could lead to improvements in de-polymerization strategies, and therefore a proper methodology and a predictive theoretical framework are required for such purpose. This work presents a complete computational study on some of the key steps of lignin polymerization mechanisms. Density Functional Theory (DFT) calculations have been performed to evaluate the most appropriate methodology and to compute the chemical structures and reaction enthalpies for the monolignol dimerization, the simplest key step that controls the polymerization. Quantum Theory of Atoms in Molecules (QTAIM) has been applied to understand the coupling reaction mechanisms, for which the radical species and transition states (TSs) involved have been characterized. The coupling that leads to the formation of the β–O–4 linkage has been theoretically reproduced according to proposed mechanisms, for which weak interactions have been found to play a key role in the arrangement of reactants. The hydrogen bond formed between the oxygen of the phenoxy radical, and the alcohol of the aliphatic chain, together with the interaction between aromatic rings, locates the reactants in a position that favors such β–O–4 linkage.

Keywords Density functional theory · lignin polymerization · QTAIM · monolignols

A. Sánchez-González
Dpto. Química Aplicada, Universidad Técnica Particular de Loja, Loja 1101608, Ecuador

F.J. Martín-Martínez
Department of Civil and Environmental Engineering, Massachusetts Institute of Technology, 77 Massachusetts Avenue, 02139 Cambridge, MA, USA Tel.: +1 617 258 8070
E-mail: fmartinm@mit.edu

J. A. Dobado
Grupo de Modelización y Diseño Molecular, Dpto. Química Orgánica, Facultad de Ciencias, Universidad de Granada, 18071 Granada, Spain

1 Introduction

Lignin [1] is the second most abundant natural polymer after cellulose and the most abundant natural material composed by aromatic moieties. [2] Around 15–30 % of plant biomass is constituted by lignin, [3] which is naturally synthesised in the cell walls of plants to provide rigidity and structural strength. [4] It also confers resistance against degradation by chemicals, enzymes or microbes, as well as recalcitrance to hydrolysis due to its cross-linking with cellulose, [5] which hinders the access of hydrolytic cellulases. Its chemical composition, its abundance, and its ubiquity have made lignin the focus of extensive research to unlock its potential as a source of aromatic compounds. [1, and references therein] However, a proper way for lignin depolymerization is still missing, partially due to a lack of understanding of the underlying mechanisms that control its polymerization. Unlocking lignin potential as source of aromatic compounds requires fundamental understanding of the polymerization mechanisms that lead to its formation, which would pave the way to reverse engineering of de-polymerization processes.

Such understanding includes the study of the radical-coupling reaction that involves the three different cinnamyl alcohols, i.e. monolignols, that compose lignin structure: *p*-coumaryl, coniferyl, and sinapyl alcohols (see Figure 1).

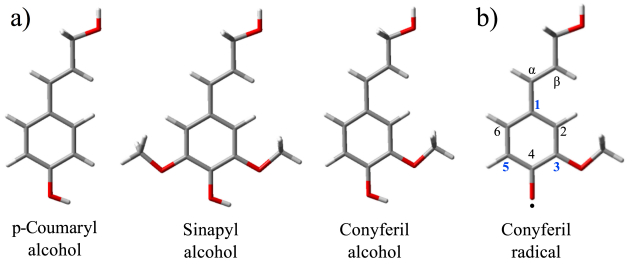

Fig. 1 Main monolignols and a radical example used in the present work. a) Chemical structure of the three most common monolignols that conform lignin structure. b) Phenoxy radical produced by the dehydrogenation of coniferyl alcohol. The common carbon labelling used for monolignols atomic positions is adopted. The positions allowed by resonance of the unpaired electron are indicated in blue, i.e. 1, 3, 5, β

In the widely assumed polymerization mechanism, laccase and peroxidase enzymes are involved in the initial dehydrogenation reaction of monolignols to produce free-radical species. [6–8] The free-radical delocalization in these species leads to resonant structures that give rise to various chemical linkages within the lignin structure. Figure 1 shows those positions allowed by resonance of the unpaired electron for a phenoxy radical, including standard atom numbering commonly adopted in monolignols. The linkages formed in lignin polymerization are then named after this standard atom numbering, and the most common among all possible connections are the so-called β–O–4, 5–5, β–5, β–β and α–linkages, as frequently described in the literature. [9] Their appearance occurs in different proportions, [10] with a noteworthy prevalence for the β–O–4 one, which is reported to have a relative abundance of 45–50 % for both softwood and hardwood lignin. [11] Other linkages have been reported to have an abundance of 18–25 % (5–5), 9–12 % (β–5), 6–8 % (α-linkages) and 3 % (β–β). In a second step that follows the generation of the radical species, lignin synthesis is assumed to happen by oxidative coupling of the corresponding monomers in their radical forms, which are incorporated to the growing polymer chain. These phenoxy radicals form part of the polymer as *p*-hydroxyphenyl (H), guayacil (G), and syringyl (S) units, which correspond to *p*-coumaryl, coniferyl, and sinapyl alcohols, respectively. The exact intermediates, transition states (TSs), and activation energies of this mechanism remain unknown.

The result of this polymerization is the well-known 3D polymer, for which experimental characterization is difficult to undertake due to the complexity of the randomly organized structure. Its low solubility hampers some chemical and physical characterization techniques, both qualitatively and quantitatively, while its difficult isolation from the polysaccharide matrix limits the amount of information available from some other experimental techniques such as NMR, Raman spectroscopy, and analytical pyrolysis. Nevertheless, the experimental studies available indicate that the molecular structure of lignin is rigid and complex, including hyper-branched domains of non-linear oligomers [12] that are organized in aggregates with a rigid core and a fluid-like surface. [13]

The lack of extensive experimental information requires the use of computational modelling and simulations to provide further insight into the structure and formation of lignin. Special attention deserves the formation of dimers, as it provides the most basic information about the polymerization mechanism. In the specific case of di-lignols, computational analyses have been mainly focused on the most common β–O–4 linkage, addressing intramolecular interactions, solvent H–bonding [14–18] and dissociation enthalpies. [19–26] Regarding other linkages, there are only few works describing the dissociation enthalpies for β–1 and β–5, [27, 28] as well as the thermal conversion of linkages during carbon-fibre production from lignin. [29,30] These computational works mainly address conformational molecular arrangements and bond-dissociation enthalpies, and only a few have tried to describe the polymerization process at a fundamental level. One of the first attempts considered the formation of one of the minor linkages, the α–O–4, [31] and calculated the electronic structure and the Fukui [32] function as a descriptor of the tendency to undergo radical reactions. Within a similar framework, the spin-density distribution of the unpaired electron in the monolignol free radicals have been described with natural bond orbital (NBO) analysis, [33] reporting a higher value of the spin density for the oxygen corresponding to the dehydrogenated alcohol, in agreement with the prevalence of β–O–4 linkage in lignin. Other works on the formation of β–O–4 provide reaction enthalpies [34] and transition structures for the coupling reactions. [35]

From all the above, no complete study is available yet on the formation mechanism, as non-covalent interactions have been ruled out in previous studies. These weak interactions, govern the initial molecular geometry of reactants and promote the emerging bonds. This has remarkable consequences, since they certainly play a crucial role in the formation of lignin. The present

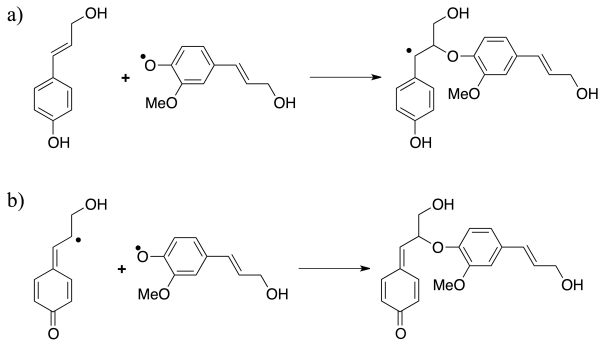

Fig. 2 Scheme of the two possible reactions proposed for the formation of β–O–4 linkage in lignin. This correspond with the mechanism 1 (a) and mechanism 2 (b) studied in the present work

work applies different methodologies, some of which have already been considered separately, and highlights the role of weak intermolecular interactions in the stabilization of the TSs during the coupling reaction. Such non-covalent interactions have been mentioned in a previous work, [36] but never emphasized as key factor during the formation β–O–4 linkages. The present study provides a clearer fundamental understanding of the bond evolution through the reaction path, and supports the prevalence of β–O–4 linkages compared to the other linkages. For consistency with established understanding of lignin polymerization, we have considered two possible reaction mechanisms as described in the literature. [34,35] One of these is a radical coupling between coumaryl alcohol, in a non-radical form, and the radical species of coniferyl and coumaryl alcohols. The other is the coupling reaction of two alcohol radicals (see Figure 2).

2 Computational details

Density functional theory (DFT) calculations were performed using Gaussian 09 computational package. [37] HSEH1PBE [38] hybrid functional has been employed together with 6-311++G(d,p) basis set to compute optimized geometries, energies, and reaction profiles of the linkage formation. This functional has been proved one of the most accurate methods to describe non-covalently interacting systems. [39] For the sake of comparison and to evaluate performance of other well-established functionals, we have performed a comparative study with B3LYP, [40,41] M062X [42] and dispersion-corrected range-separated double hybrid functional (ωB97XD) [43] (see Supporting Information). There exist small differences between the different computational methods regarding the spin densities on the three monolignol radicals and their link to the reactivity of a particular site. Overall, it turns out that both O and C_1 are equally reactive sites within the radical systems.

Zero-point energy corrections (ZPE) were applied in all cases to provide accurate energy values. Stationary points and TSs were characterized by calculating the eigenvalues of the second-derivative matrix, i.e. Hessian. None of the energy minima showed any imaginary frequencies, while TSs presented a single-point imaginary frequency. TSs optimal geometry and its associated energy were determined from a relaxed scan along the reaction coordinate.

The electron-spin density was evaluated with natural bond orbital (NBO) analysis [44] and the isosurfaces of the spin densities were plotted with the AIMAll software. [45]

Spin contamination in a unrestricted wave function has been evaluated by the deviation of the of <S2> with respect to the expected value, e.g. 0.75 for a doublet, s(s+1), where s equals 1/2 times the number of unpaired electrons. These deviations can be considered negligible in organic molecules [46] if the value of <S2> differs from s(s+1) by less than 10%. For the radical species involved in the study, and using the HSEH1PBE functional, the deviation is aroun 5% (see supporting information).

Non-covalent interactions were analyzed using the non-covalent interaction (NCI) index [47] and plotted with AIMAll software. NCI index enables the identification of stabilizing non-covalent interactions, by representing the reduced gradient of the electron density mapped with the second value of the Hessian.

The topology of the electron density was analyzed with quantum theory of atoms in molecules (QTAIM), [48] also using AIMAll [45] software.

3 Results and discussion

3.1 Electron-spin densities for monolignol radicals

The formation of phenoxy radicals from the main monolignols constitutes the first step of the radical-coupling reaction that leads to lignin biosynthesis. To characterize the free-radical delocalization in the radical species, we report spin densities extracted from the unrestricted wavefunction analysis with HSEH1PBE/6-311++G(d,p) for the three main alcohol radicals (see Figure 3).

The results indicate a similar trend for the three different alcohols, where the relevance of the radical O atom in the formation of β–O–4 linkages is clearly pointed out. High spin-density values in this oxygen (0.274–0.312), suggest this position as the most reactive site in the radical. In addition, C_1 follows the O atoms as a possible reactive site in the radical species.

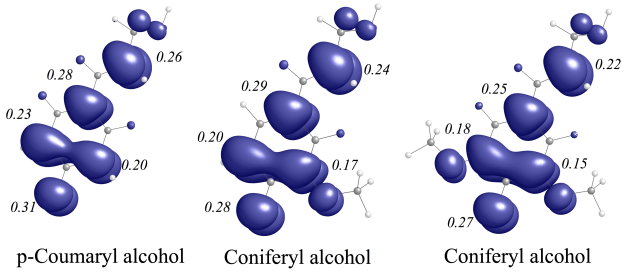

Fig. 3 Electron spin density plots for the monolignol radicals involved in lignin polymerization, plotted at s=0.001 value, and the spin density numerical values for the main atomic positions, computed with HSEH1PBE/6-311++G(d,p)

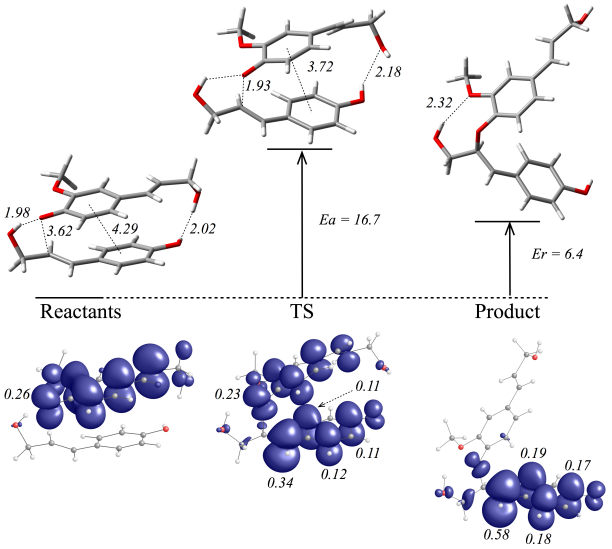

Fig. 4 Reaction energy profile for the radical coupling reaction of coumaryl alcohol with coniferyl phenoxy radical alcohol, together with the optimized geometries for reactants, TS and products. The electron spin densities (s=0.001) for the main species and the spin density numerical values are also shown, all of them computed with HSEH1PBE/6-311++G(d,p). The activation Energy (E_a) and the energy of the products relative to the reactants are shown in Kcal mol^{-1}. The most relevant distances are also indicated, in Å

This is in disagreement with the relative low abundance reported for C_1–linkages in lignin, [49] which suggests that C_1–linkages may occur under certain specific circumstances once the α and β positions are already saturated. [50] Other positions such as C_β, C_3, and C_5 are shown to be equally reactive according to spin density values, but less reactive than O and C_1 atoms. It is important to note that even though the C_3 and C_5 positions are suitable to allocate a free-radical electron, the presence of MeO groups is a steric impediment for the radical-coupling reaction in coniferyl and sinapyl alcohols. Therefore, C_β and dehydrogenated O atoms are the most favourable sites for radical coupling.

3.2 Mechanism 1: coupling reaction between a monolignol and a radical monolignol

3.2.1 Geometries, spin-densities and reaction profiles

The first mechanism (β–O–4 coupling reaction) under consideration involves radical and non-radical monolignol molecules. Figure 4 depicts the energy profile for this first mechanism, where the coumaryl alcohol undergoes radical coupling with the coniferyl alcohol radical. According to DFT calculations, this mechanism implies two possible geometries for the TS (see Supporting Information). The presence of H–bond between the H atom of the aliphatic alcohol of the coumaryl molecule and the O atom of the phenoxy radical in one of the possible TSs decreases the activation energy around 4 Kcal mol^{-1}. This has been calculated only to evaluate the influence of H bonding in the stabilization, emphasizing the relevance of this weak interaction in the reaction mechanism. Also, our results indicate that the MeO group in the radical monolignol yields a destabilization of the TS and increases the activation energy (see Supporting Information). This destabilization is originated by a so-called pull effect of the MeO group in the relative stability of the phenoxy radical, which contributes to the delocalization of the unpaired electron. Indeed, the spin densities in Figure 3 support this idea, since the values for the O atom have been decreased by the presence of MeO groups. The trend is the same for Gibbs free energies, being the Gibbs free activation energy ($\Delta G^{\ddagger}$) equal to 18.0 Kcal mol^{-1} and the Gibbs free reaction energy (ΔG_r) to 5.0 Kcal mol^{-1}. The entropic effect is remarkable, but it does not make a difference in the reaction mechanism already described.

The geometrical arrangements depicted in Figure 4 also remark the proximity of the O atom of the radical monolignol to the C_β of the coumaryl alcohol in the reactants. The geometries reveal a parallel orientation of the aromatic rings, suggesting π–π interactions in addition the already described H–bonding. From the methodological point of view, this result emphasizes the importance of including dispersion-corrections in the functional when aromatic rings are present, e.g. B3LYP only describes the H–bonding (see Supporting Information). The geometrical arrangement originated by the presence of these π–π interactions also favors the proximity between the spin densities of O and C_β atoms in the TS that lead the formation of a β–O–4 linkage. In the case of the O atom of the phenoxy radical monolignol the spin density has indeed higher value (0.264). However, it is reduced for the TS (0.232), for which C_α position in the coumaryl alcohol increases (0.343).

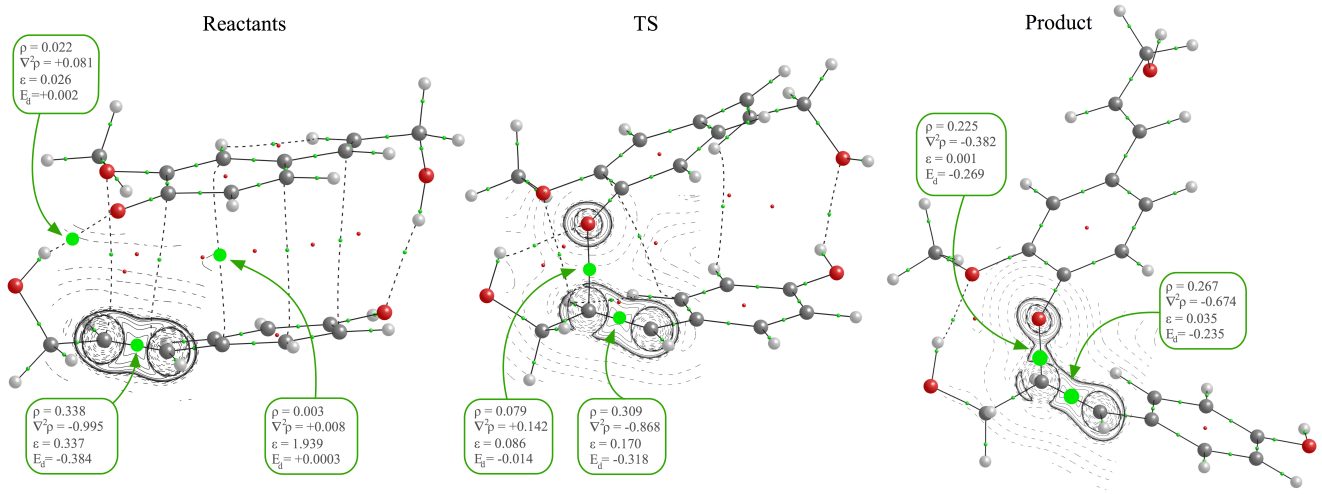

Fig. 5 Bonding scheme and $\nabla^2\rho$(r) plots for reactants, TS and products for the coupling reaction of coumaryl monolignol with of coniferyl alcohol radical. The thick lines represents atomic interaction paths joining the nuclei. Green points represents BCPs. The most relevant BCPs for the reaction have been highlighted, indicating their characteristic values of Laplacian ($\nabla^2\rho$), electron density (ρ), and ellipticity. Red points represents ring critical points (RCPs). Thin solid lines represents charge concentration zones, negative values for $\nabla^2\rho$(r). Thin dotted lines charge depletion zones, positive values of $\nabla^2\rho$(r). All the values and geometries are computed at HSEH1PBE/6-311++G(d,p) level

This increment in the spin density at C_α position is even larger in the product, with a value of 0.583, which points out the C_α position as the most reactive and suitable atom for a subsequent oxidative coupling.

3.2.2 Topology of the electron density and non-covalent interactions

Further analysis is provided by analyzing the topology of the electron density for reactants, TSs and products with QTAIM. The electron density at the bond critical point (BCP) describes the strength of the bond, as it measures the electron population in the area between two atoms, quantifying the degree of bond multiplicity. Additionally, the electron-energy density (E_d) at this point characterizes the stability of the bond. Negative values for the E_d represent more stabilized interactions, while values close to zero are characteristic of weak interactions and low density critical points. Figure 5 depicts the topology of the electron density and the values for the main descriptors characterizing the BCPs for the species involved in the reaction between coumaryl alcohol and the coniferyl alcohol radical. The values associated to the C_α–C_β BCP agree with C–C double bonds, where ρ(r), E_d and ϵ present high values, namely 0.338 (e^- a_0^{-3}), -0.384 (Hartree a_0^{-3}) and 0.337, respectively.

For the reactants, several BCPs associated to weak interactions have been found. In fact, two BCPs corresponding to H–bonds are present in the structure. These bonds are characterized by low electron density, e.g. 0.022 (e^- a_0^{-3}), positive value of the Laplacian and low positive value for the E_d, e.g. 0.002 (Hartree a_0^{-3}). This H–bonding is responsible for the proximity between the deprotonated O atom of the radical monolignol and the C_β of the coumaryl alcohol. Additionally, there are five BCPs connecting the two molecular planes which are responsible of the π–π stacking. Such BCPs are characterized by very low value of ρ(r), e.g. 0.003 (e^- a_0^{-3}), positive values for the Laplacian, e.g. 0.008 (e^- a_0^{-5}) and low positive E_d values, e.g 0.0003 (Hartree a_0^{-3}). Despite the low values of these BCPs, the stabilization provided by them plays a key role in the behavior and chemical structure of the reactants, as it has been also proved previously in other C–C interactions. [51]

Regarding the TS, the bonding scheme changes but remains more similar to the reactants than to the products. Most of the BCPs corresponding to weak interactions between the two molecular planes have vanished for the TS. Instead, a weak C_β–O bond is shown, with a BCP characterized by low values of ρ and E_d, 0.079 e^- a_0^{-3} and -0.014 Hartree a_0^{-3}, respectively. The C_α–C_β bond has the expected values of a double bond, i.e. high electron density, ρ = 0.309 e^- a_0^{-3}, and a high negative value of E_d = -0.318. Only the ϵ values have decreased to 0.189. These results imply that the electronic structure of the TS is more similar to the electronic structure in the reactants than in the products. These results suggest that the step from the TS to the products implies more significant changes at the atomic level than the formation of the TS, and therefore going from TS to products is the limiting step. Forming the TS is easier

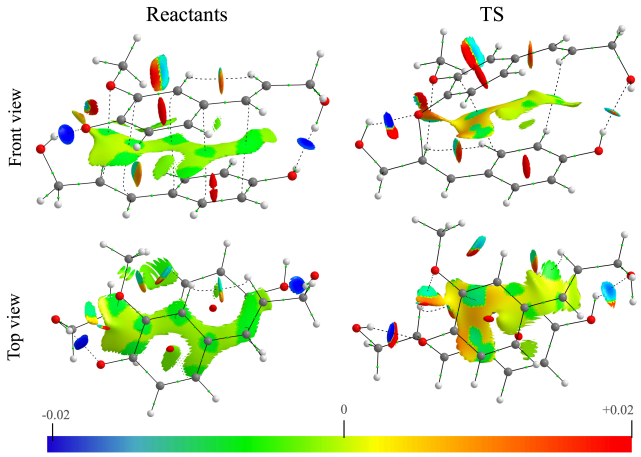

Fig. 6 NCI index plots with gradient isosurfaces (s = 0.5 au) for reactants and TS in the coupling reaction between coumaryl alcohol and coniferyl radical alcohol

from the ρ(r) standpoint, and once the reaction goes beyond the TS to form the products, it is more difficult to reverse, since it implies major changes in the electronic structure. This is also supported by the negative values of the Laplacian (solid lines in the contour maps), as shown for the C_α–C_β bond in the TS.

Further analysis of the weak interactions involved in the reaction mechanism, is provided by the NCI index, [47]. Figure 6 shows the representation of the NCI index computed for the reactants and TSs. Blue and pale green indicate negative values which implies stabilizing interactions; being yellow and red ones positive values for destabilizing interactions. For the reactant complex, there is a large zone between the two molecular planes with a negative value for NCI index (green) located near the low density BCPs, which implies π–π interactions along the aromatic rings. In addition, the H–bonds of both OH groups present the expected most negative value for the NCI index, being the most stabilizing weak interactions in this molecular system. The structure of the TS yielded a similar NCI index distribution. The only difference is shown between the two aromatic rings, were the isosurface has been slightly distorted due to the separation of the radical alcohol. Both reactants and TS, show negative values for NCI index between the molecular planes, which agree with low-density BCPs connecting the aromatic regions. This analysis corroborates that the weak interactions ruling the geometry of reactants are maintained for the TS and lead the coupling process along the reaction path.

3.3 Mechanism 2: coupling reaction between radical coumaryl and radical coniferyl monolignols

The reaction profile has been also described for the radical coupling between the radical coumaryl monolignol and the radical coniferyl alcohol. The fully optimized geometries for the reactants are quite similar to the previous mechanism, where the two aromatic systems are facing each other with a center-to-center distance of 3.98 Å (see Figure 7). Concerning Gibbs free energies, the activation energy ($\Delta G^{\ddagger}$) and the Gibbs free reaction energy (ΔG_r) confirm the trend, with values of 18.1 Kcal mol^{-1} and 11.7 Kcal mol^{-1} respectively. The entropic effect is remarkable, but it does not make a difference in the reaction mechanism already described. Additionally, the H–bond formed with the alcohol of the aliphatic chain helps to locate the O atom on top of the C_β. Here again such H–bond occurs with the dehydrogenated O atom of the coniferyl alcohol, and not with the O atom corresponding to the MeO group. As opposed to mechanism 1, unexpectedly, the TS found corresponds to the formation of a C–C bond between the two aromatic rings, C_5–C_1 linkage (see Figure 7), and no TS was found for the β–O–4 linkage. In this TS, the H–bond contributes to a propitious stabilizing interaction. Regarding the new C–C bond formed via this mechanism, the presented bond distance is 1.98 Å.

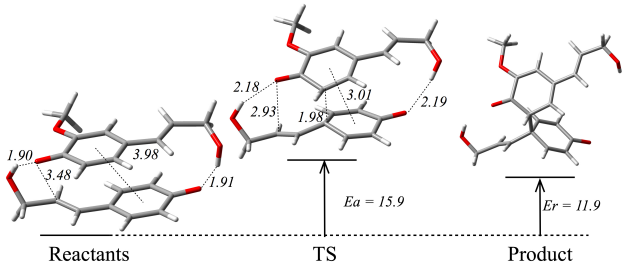

Fig. 7 Energy profile (Kcal mol^{-1}) and selected distances (Å) for the radical coupling reaction of radical coumaryl alcohol with phenoxy radical coniferyl alcohol, computed at HSEH1PBE/6-311++G(d,p) level
f

The different trend during the formation of the linkage in which the monolingol has already been dehydrogenated and it is in radical form can be understood attending to the spin-density population shown for C_1 (see Figure 3), where the spin density in this C atom reaches high values. Taking into account the geometrical arrangement for the reactants, the same orientation depicted above is presented, the co-facial disposition of the aromatic rings, and the H–bond formed between the O atom of the coniferyl radical monolignol and the OH group, allows the O atom to be close to C_β. On the

other hand, at the same time C_1 and C_5 atoms are also faced. As can be seen (see Figure 8), this geometrical disposition between both radicals, allows the proximity between the spin densities for the C_1 of the coumaryl radical monolignol and the C_3 and C_5 corresponding to coniferyl radical monolignol. Furthermore, the value for C_1 in the coumaryl radical is even higher than for the oxygen spin density, This proximity and the corresponding values for the spin density, allows the C–C bond formation. The reaction for a radical coupling between two radical monolignos shows the same results for ωB97XD functional, resulting a TS corresponding to a C_1-C_5 linkage formation (See Figure 22 in supporting information).

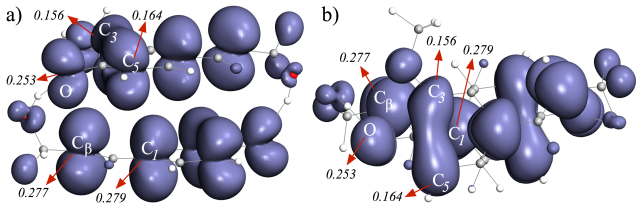

Fig. 8 Plotted spin densities (s=0.001) computed at HSEH1PBE/6-311++G(d,p) theoretical level, for the reactants arrangement between the two radical alcohols, front view and top view

To gain insight into the role played by the electron density in this reaction, QTAIM analyses have been performed for reactants and TS. Figure 9 shows bonding scheme and the Laplacian contour map plotted on a plane containing C_5, C_1 and C_β atoms. Again, as in the previous mechanism, in the reactants arrangement four BCPs are showed connecting both molecular planes and two BCPs for the H–bonds. Regard to the TS, a BCP is shown for the incipient bond between the carbon atoms belonging to the aromatic rings. In addition, the charge-concentration zones corresponding to both carbon atoms show lobed shapes along the bond direction. On the other hand, no BCP is shown between the O atom and the C_β. Figure 9 also presents the corresponding values for BCP of the incipient bond between C_1 and C_5 in the TS. The values presented for the $\rho(r)$ and E_d, are 0.091 (e^- a_0^{-3}) and -0.032 (Hartree a_0^{-3}), respectively. These values being quite similar to the BCP for the C_β–O linkage in the TS shown above in the previous mechanism. In Figure 10, NCI isosurfaces are presented for the reactants and TS. For the reactants, in this case, the area of negative values (pale green) between two radical alcohols has been increased regard to the previous mechanism studied above, being these areas the surrounding space of the low-density BCPs connecting the aromatic moieties of both molecules. Again the most stabilizing interaction corresponds to both H–bonds presenting high negative values. For the TS structure, the isosurface presents remarkable changes. In this TS the stabilizing interaction area has been reduced and distorted due to the formation of C_1–C_5 linkage. However, in the TS still remains an important non-covalent interaction, considering the negative values for NCI isosurface between both molecular moieties and the H–bonds represented by pale blue areas.

4 Conclusions

We have provided fundamental understanding of the non-covalent interactions, and molecular conformation that lead the formation of the most abundant linkage present in lignin, the β–O–4. Using DFT, QTAIM and NCI index calculations, we have characterized reactants, TSs and products for the two main accepted mechanisms of lignin polymerization.

According to our results, the H–bonding and π–π interactions presented between the reactants, locate the C_β and the O atom in a geometrical arrangement that favors the formation of the β–O–4. Such interactions constitute the main contribution to the prevalence of this linkage. For the proposed mechanisms, taking into account the above-mentioned results, mainly the β–O–4 linkage occurs, through a coupling between a radical monolignol and non-deprotonated monolignol or a unit previously assembled in the biopolymer. The reaction between two radical units could lead to C_1–linkages and such linkages are the most infrequent in natural lignin.

For the systems studied, the geometries and conformations depend on the interaction of different groups, aromatic and polar moieties. The consideration of non-covalent interactions between the moieties present in the reactants is mandatory to accurately describe the systems studied.

Acknowledgements This work was financed by Proyecto Prometeo, Secretaría de Educación Superior, Ciencia, Tecnología e Innovación of the Republic of Ecuador. We also thank the "Centro de Servicios de Informática y Redes de Comunicaciones" (CSIRC) (UGRGrid), University of Granada and Universidad Técnica Particular de Loja for providing computing time. Mr. David Nesbitt reviewed the English version of the manuscript. We want to thank Dr. Santiago Melchor their help in the management of computing resources.

References

1. Calvo-Flores FG, Dobado JA, Isac-Garcia J, Martin-Martinez FJ (2015) Lignin and lignangs as renovable raw

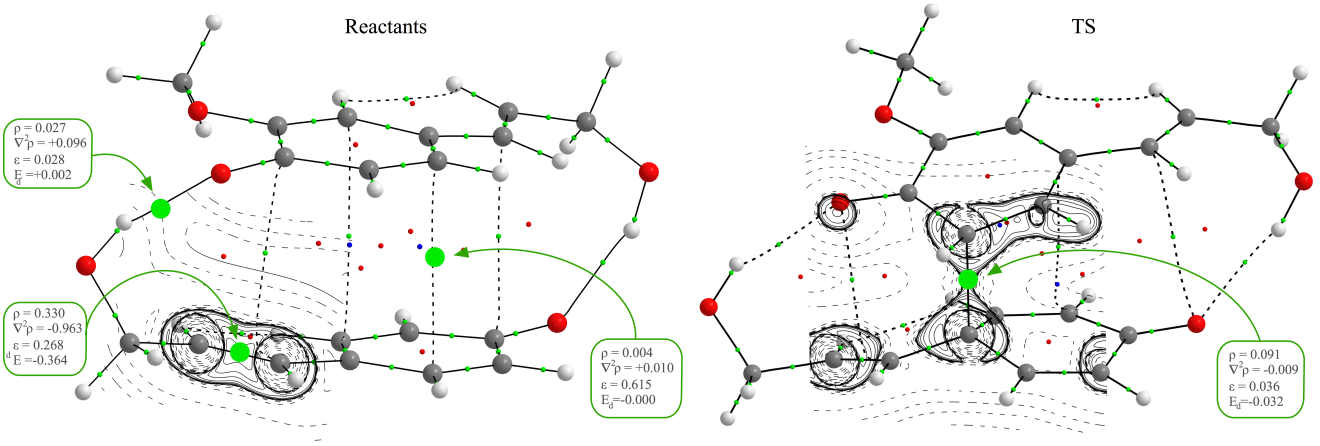

Fig. 9 Bonding scheme and $\nabla^2\rho(\mathrm{r})$ plots for reactants and TS forming the C_1 linkage. The thick lines represent bond paths joining the nuclei, green points represent the BCPs, and red points, ring critical points (RCPs). Blue points are cage critical points (CCP) Thin solid lines represent charge concentration zones, negative values for $\nabla^2\rho(\mathrm{r})$. Dotted lines represent charge depletion zones, positive values for $\nabla^2\rho(\mathrm{r})$.

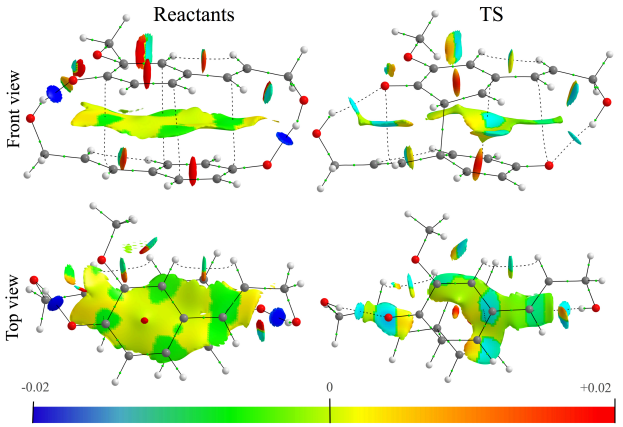

Fig. 10 Gradient isosurfaces (s = 0.5 au) for reactants and TS in the coupling reaction between coumaryl alcohol radical and coniferyl alcohol radical

materials: chemistry, technology and applications. Wiley-VCH, Weinheim
2. O′Sullivan AC (1997) Cellulose: the structure slowly unravels. Cellulose 4:173–207. doi: 10.1023/A:1018431705579
3. Bonawitz ND, Chaple C (2010) The genetics of lignin biosynthesis: connecting genotype to phenotype. Annu Rev Genet 44:337–363. doi: 10.1146/annurev-genet-102209-163508
4. Whetten RW, MacKay JJ, Sederoff RR (1998) Recent advances in understanding lignin biosynthesis. Annu Rev Plant Physiol Plant Mol Biol 49:585–609. doi: 10.1146/annurev.arplant.49.1.585
5. Balakshin M, Capanema E, Gracz H, Chang HM, Jameel H (2011) Quantification of lignin-carbohydrate linkages with high-resolution NMR spectroscopy. Planta 233:1097–1110. doi: 10.1007/s00425-011-1359-2
6. Freudenberg K (1965) Lignin: its constitution and formation from *p*-hydroxycinnamyl alcohols. Science 148:595–600. doi: 10.1126/science.148.3670.595
7. Aoyama W, Sasaki S, Matsumura S, Mitsunaga T, Hirai H, Tsutsumi Y, Nishida T (2002) Sinapyl alcohol-specific peroxidase isoenzyme catalyzes the formation of the dehydrogenative polymer from sinapyl alcohol. J Wood Sci 48:497–504. doi: 10.1007/BF00766646
8. Kobayashi T, Taguchi H, Shigematsu M, Tanahashi M (2005) Substituent effects of 3,5-disubstituted *p*-coumaryl alcohols on their oxidation using horseradish peroxidase–H_2O_2 as the oxidant. J Wood Sci 51:607–614. doi: 10.1007/s10086-005-0702-2
9. Boerjan W, Ralph J, Baucher M (2003) Lignin biosynthesis. Annu Plant Biol 54:519–546. doi: 10.1146/annurev.arplant.54.031902.134938
10. Chakar FS, Ragaukas AJ (2004) Review of current and future softwood kraft lignin process chemistry. Ind Crops Prod 20:131–141. doi: 10.1016/j.indcrop.2004.04.016
11. Sakakibara A (1980) A structural model of softwood lignin. Wood Sci Technol 14:89–100. doi: 10.1007/BF00584038
12. Harton SE, Pingali SV, Nunnery GA (2012) Evidence for complex molecular architectures for solvent-extracted lignins. ACS Macro Lett 1:568–573. doi: 10.1021/mz300045e
13. Petridis L, Pingali SV, Urban V, Heller WT, O′Neill HM, Foston M, Ragauskas A, Smith JC (2011) Self-similar multiscale structure of lignin revealed by neutron scattering and molecular dynamics simulation. Phys Rev E83:061911. doi: 10.1103/PhysRevE.83.061911
14. Besombes S, Robert D, Utille J, Taravel FR, Mazeau K (2003) Molecular modeling of lignin *β*–O–4 model compounds. Comparative study of the computed and experimental conformational properties for a guaiacyl *β*–O–4 dimer. Holzforschung 57:266–274. doi: 10.1515/HF.2003.040
15. Besombes S, Robert D, Utille J, Taravel FR, Mazeau K (2003) Molecular modeling of syringyl and *p*-hydroxyphenyl *β*–O–4 dimers. Comparative study of the computed and experimental conformational properties of lignin *β*–O–4 model compounds. J Agric Food Chem 51:34–42. doi: 10.1021/jf0206668
16. Durbeej B, Eriksson LA (2003) A density functional theory study of coniferyl alcohol intermonomeric cross linkages in lignin: three-dimensional structures, stabilities and the thermodynamic control hypothesis. Holzforschung 57:150–164. doi: 10.1515/HF.2003.024

17. Besombes S, Utille J, Mazeau K, Robert D, Taravel FR (2004) Conformational study of a guaiacyl β-O-4 lignin model compound by NMR. Examination of intramolecular hydrogen bonding interactions and conformational flexibility in solution. Magn Reson Chem 42:337–347. doi: 10.1002/mrc.1317
18. Besombes S, Mazeau K (2004) Molecular dynamics simulations of a guaiacyl β–O–4 lignin model compound: examination of intramolecular hydrogen bonding and conformational flexibility. Biopolymers 73:301–315. doi: 10.1002/bip.10587
19. Beste A, Buchanan III AC (2009) Computational study of bond dissociation enthalpies for lignin model compounds. Substituent effects in phenethyl phenyl ethers. J Org Chem 74:2837–2841. doi: 10.1021/jo9001307
20. Elder T (2010) A computational study of pyrolysis reactions of lignin model compounds. Holzforschung 64:435–440. doi: 10.1515/hf.2010.086
21. Younker JM, Beste A, Buchanan III AC (2011) Computational study of bond dissociation enthalpies for substituted β–O–4 lignin model compounds. ChemPhysChem 12:3556–3565. doi: 10.1002/cphc.201100477
22. Kim S, Chmely SC, Nimlos MR, Bomble YJ, Foust TD, Paton RS, Beckham GT (2011) Computational study of bond dissociation enthalpies for a large range of native and modified lignins. J Phys Chem Lett 2:2846–2852. doi: 10.1021/jz201182w
23. Beste A, Buchanan III AC (2013) Computational investigation of the pyrolysis product selectivity for α–hydroxy phenethyl phenyl ether and phenethyl phenyl ether: analysis of substituent effects and reactant conformer selection. J Phys Chem A 117:3235–3242. doi: 10.1021/jp4015004
24. Huang J, Liu C, Tong H, Li W, Wu D (2014) A density functional theory study on formation mechanism of CO, CO_2 and CH_4 in pyrolysis of lignin. Comput Theor Chem 1045:1–9. doi: 10.1016/j.comptc.2014.06.009
25. Huang J, Liu C, Wu D, Tong H, Ren L (2014) Density functional theory studies on pyrolysis mechanism of β–O–4 type lignin dimer model compound. J Anal Appl Pyrolysis 109:98–106. doi: 10.1016/j.jaap.2014.07.007
26. Janesko BG (2014) Acid-catalyzed hydrolysis of lignin β–O–4 linkages in ionic liquid solvents: a computational mechanistic study. Phys Chem Chem Phys 16:5423–5433. doi: 10.1039/C3CP53836B
27. Younker JM, Beste A, Buchanan III AC (2012) Computational study of bond dissociation enthalpies for lignin model compounds: β–5 Arylcoumaran. Chem Phys Lett 545:100–106. doi: 10.1016/j.cplett.2012.07.017
28. Huang J, He C, Liu C, Tong H, Wu L, Wu S (2015) A computational study on thermal decomposition mechanism of β–1 linkage lignin dimer. Comput Theor Chem 1054:80–87. doi: 10.1016/j.comptc.2014.12.007
29. Beste A (2014) ReaxFF study of the oxidation of lignin model compounds for the most common linkages in softwood in view of carbon fiber production. J Phys Chem A 118:803–814. doi: 10.1021/jp410454q
30. Beste A, Buchanan III AC (2011) Kinetic analysis of the phenyl-shift reaction in β–O–4 lignin model compounds: a computational study. J Org Chem 76:2195–2203. doi: 10.1021/jo2000385
31. Watts HD, Mohamed MNA, Kubicki JD (2011) Evaluation of potential reaction mechanisms leading to the formation of coniferyl alcohol α–linkages in lignin: a density functional theory study. Phys Chem Chem Phys 13:20974–20985. doi: 10.1039/c1cp21906e
32. Ayers PW, Yang W, Bartolotti LJ (2009) The Fukui function in Chemical reactivity theory: a density functional view. (Ed: Chattaraj PK), CRC Press, New York, pp. 255–267
33. Durbeej B, Erikson LA (2003) Spin distribution in dehydrogenated coniferyl alcohol and associated dilignol radicals. Holzforschung 57:59–61. doi: 10.1515/HF.2003.009,
34. Sangha AK, Parks JM, Standaert RF, Ziebell A, Davis M, Smith JC (2012) Relative binding affinities of monolignols to horseradish peroxidase. J Phys Chem B 116:4760–4768. doi: 10.1021/acs.jpcb.6b00789
35. Durbeej B, Eriksson LA (2003) Formation of β–O–4 lignin models – a theoretical study. Holzforschung 57:466–478. doi: 10.1515/HF.2003.070
36. Chen Y, Sarkanen S (2010) Macromolecular replication during lignin biosynthesis. Phytochemistry 71:453–462. doi: 10.1016/j.phytochem.2009.11.012
37. Frisch MJ, Trucks GW, Schlegel HB, Scuseria GE, Robb MA, Cheeseman JR, Scalmani G, Barone V, Mennucci B, Petersson GA, Nakatsuji H, Caricato M, Li X, Hratchian HP, Izmaylov AF, Bloino J, Zheng G, Sonnenberg JL, Hada M, Ehara M, Toyota K, Fukuda R, Hasegawa J, Ishida M, Nakajima T, Honda Y, Kitao O, Nakai H, Vreven T, Montgomery JA Jr, Peralta JE, Ogliaro F, Bearpark M, Heyd JJ, Brothers E, Kudin KN, Staroverov VN, Kobayashi R, Normand J, Raghavachari K, Rendell A, Burant JC, Iyengar SS, Tomasi J, Cossi M, Rega N, Millam JM, Klene M, Knox JE, Cross JB, Bakken V, Adamo C, Jaramillo J, Gomperts R, Stratmann RE, Yazyev O, Austin AJ, Cammi R, Pomelli C, Ochterski JW, Martin RL, Morokuma K, Zakrzewski VG, Voth GA, Salvador P, Dannenberg JJ, Dapprich S, Daniels AD, Farkas Ö, Foresman JB, Ortiz JV, Cioslowski J, Fox DJ (2009) Gaussian 09 revision B.01. Gaussian Inc., Wallingford
38. Henderson TM, Izmaylov AF, Scalmani G, Scuseria GE (2009) Can short-range hybrids describe long-range-dependent properties? J Chem Phys 131:044108. doi: 10.1063/1.3185673
39. Remya, K. and Suresh, C. H. (2013) Which density functional is close to CCSD accuracy to describe geometry and interaction energy of small noncovalent dimers? A benchmark study using Gaussian09. J Comput Chem 34:1341–1353. doi: 10.1002/jcc.23263
40. Becke AD (1993) Density-functional thermochemistry. III. The role of exact exchange. J Chem Phys 98:5648–5652. doi: 10.1063/1.464913
41. Lee C, Yang W, Parr RG (1988) Development of the Colle-Salvetti correlation-energy formula into a functional of the electron density. Phys Rev B 37:785–789. doi: 10.1103/PhysRevB.37.785
42. Zhao Y, Truhlar DG (2008) The M06 suite of density functionals for main group thermochemistry, thermochemical kinetics, noncovalent interactions, excited states, and transition elements: two new functionals and systematic testing of four M06-class functionals and 12 other functionals. Theor Chem Account 120:215–241. doi: 10.1007/s00214-007-0310-x
43. Chai JD, Head-Gordon M (2008) Long-range corrected hybrid density functionals with damped atom-atom dispersion corrections. Phys Chem Chem Phys 10:6615–6620. doi: 10.1039/b810189b
44. Reed AE, Curtiss LA, Weinhold F (1988) Intermolecular interactions from a natural bond orbital, donor-acceptor viewpoint. Chem Rev 88:889–926. doi: 10.1021/cr00088a005
45. AIMAll (Version 15.09.27), Todd AK, Gristmill TK Software, Overland Park KS, USA, 2015 (aim.tkgristmill.com).

46. Young D, (2001) Computational Chemistry: A practical Guide for Applying Techniques to Real World Problems. John Wiley and Sons.
47. Johnson ER, Keinan S, Mori-Sánchez P, Contreras-García J, Cohen AJ, Yang W (2010) Revealing noncovalent interactions J Amer Chem Soc 132:6498–6506. doi: 10.1021/ja100936w
48. Bader RFW (1990) Atoms in molecules: a quantum theory. Clarendon Press, Oxford U.K.
49. Sjöström E (1981) Wood chemistry: fundamentals and applications. Academic Press, New York
50. Setälä H, Pajunen A, Rummakko P, Sipilä J, Brunow G (1999) A novel type of spiro compound formed by oxidative cross coupling of methyl sinapate with a syringyl lignin model compound. A model system for the β–1 pathway in lignin biosynthesis. J Chem Soc Perkin Trans 1 461–464. doi: 10.1039/A808884E
51. Alkorta I, Blanco F, Elguero J, Dobado JA, Melchor A, Vidal I (2009) Carbon$\cdots$carbon weak interactions. J Phys Chem A. 113:8387–8393. doi: 10.1021/jp903016e